Relationships between Water Wettability and Ice Adhesion

Adam J. Meuler,[1,2] J. David Smith,[3] Kripa K. Varanasi,[3] Joseph M. Mabry,[1] Gareth H. McKinley,[3*] and Robert E. Cohen[2*]

[1] Space and Missile Propulsion Division, Air Force Research Laboratory, Edwards Air Force Base, California 93524

[2] Department of Chemical Engineering, Massachusetts Institute of Technology, Cambridge, Massachusetts 02139

[3] Department of Mechanical Engineering, Massachusetts Institute of Technology, Cambridge, Massachusetts 02139

Abstract

Ice formation and accretion may hinder the operation of many systems critical to national infrastructure, including airplanes, power lines, windmills, ships, and telecommunications equipment. Yet despite the pervasiveness of the icing problem, the fundamentals of ice adhesion have received relatively little attention in the scientific literature and it is not widely understood which attributes must be tuned to systematically design "icephobic" surfaces that are resistant to icing. Here we probe the relationships between advancing/receding water contact angles and the strength of ice adhesion to bare steel and twenty-one different test coatings (~200-300 nm thick) applied to the nominally smooth steel discs. Contact angles are measured using a commercially available goniometer while the average shear strengths of ice adhesion are evaluated with a custom-built laboratory-scale adhesion apparatus. The coatings investigated are comprised of commercially available polymers and fluorinated polyhedral oligomeric

silsesquioxanes (fluorodecyl POSS), a low surface energy additive known to enhance liquid repellency. Ice adhesion strength correlates strongly with the practical works of adhesion required to remove liquid water drops from the surfaces (i.e., with the quantity $[1 + \cos \theta_{rec}]$), and the average shear strength of ice adhesion was reduced by as much as a factor of 4.2 when bare steel discs were coated with fluorodecyl POSS- containing materials. We argue that any further appreciable reduction in ice adhesion strength will require textured surfaces, as no known materials exhibit receding water contact angles on smooth/flat surfaces that are significantly above those reported here (i.e., the values of $[1 + \cos \theta_{rec}]$ reported here have essentially reached a minimum for known materials).

Introduction

The formation and accretion of ice on exposed surfaces may hinder the operational performance of, for example, aircraft,[1-3] helicopters,[2, 4] ships,[2, 5] offshore oil platforms,[6] power lines,[2, 7] wind turbines,[8, 9] locks and dams,[2, 10] and telecommunications equipment.[2, 11, 12] Often some sort of de-icing protocol, such as spraying aircraft with glycol-based fluids,[1, 13, 14] is used to mitigate complications due to icing by removing ice that has formed on a surface. Such processes are suboptimal, however, because they require frequent application (e.g., spraying a plane before each cold weather departure), may be expensive,[10] and often have detrimental environmental consequences.[1, 13, 14] A related strategy utilizes "sacrificial" coatings (e.g., silicone grease) that remove ice particulates as they are shed from treated surfaces.[3, 15, 16] While this approach has proven effective in reducing ice adhesion,[3, 15, 16] these sacrificial coatings, similar to de-icing protocols, may negatively impact the environment and require periodic re-application,

2

although some recently developed sol-gel systems that slowly release freezing point depressants may significantly reduce the required frequency of re-application.[17, 18] A more appealing and universal approach is to design surfaces to which ice minimally adheres, ideally such that the ice debonds under its own weight or due to natural factors such as wind. The elucidation of the mechanism(s) of ice adhesion and the requisite surface properties to minimize ice-substrate interactions should facilitate the successful development of such "icephobic" coatings. Researchers have pursued such an understanding for more than 50 years, greatly increasing knowledge of ice adhesion phenomena.[2, 3, 5, 7, 8, 10-12, 19-58] A few of these earlier publications include extensive discussion of the previous literature detailing the relationships between ice adhesion and water wettability,[2, 34] a focus of this manuscript. Yet despite these research efforts, clearly defined design principles for the preparation of icephobic surfaces have remained elusive.

A common theme in ice adhesion research has been the comparison of ice adhesion strength and water wettability (surface hydrophobicity). Often this comparison has taken the form of a plot or tabular listing of measured ice adhesion strength as a function of the "water contact angle."[23-25, 31, 34, 42, 43, 51, 53] Data presented in this manner do not always follow a common trend, however; some groups have reported that ice adhesion decreases with increasing water contact angle,[34, 43, 51] while others have found little relation between the two parameters.[23-25, 31, 53] Petrenko and Whitworth compiled ice adhesion and water contact angle data from several research groups on a single plot and found that, while the ice adhesion strength generally decreased with increasing water contact angle, significant scatter was present in the data; reported ice adhesion strengths

varied by as much as a factor of ten for some samples with comparable water contact angles.[42]

We believe the lack of clear trends in these data derives from the use of a single, presumably static equilibrium, water contact angle as a quantitative measure of the water wettability. A number of groups have pointed out that a single contact angle does not adequately characterize the wettability of a surface as, for example, the angle of tilt required to induce sliding of sessile liquid drops does not correlate with any one contact angle.[31, 59-61] Gao and McCarthy noted that a more complete description of liquid wettability (or conversely, repellency) could be provided by separately considering shear and tensile phenomena.[60, 61] Drop sliding is inherently a shearing process; the minimum angle of tilt (α) at which a sessile droplet will spontaneously move can be predicted using an equation proposed by Furmidge:[62]

$$(mg \, / \, w) \sin(\alpha) = \gamma_{LV} (\cos \theta_{rec} - \cos \theta_{adv}) \quad\quad\quad (1)$$

where m is the mass of the drop, g is the gravitational constant, w is the width of the drop perpendicular to the drop sliding direction, γ_{LV} is the liquid-vapor surface tension of the liquid, and θ_{rec} and θ_{adv} are the receding and advancing contact angles of the liquid on the substrate, respectively. The dimensionless solid-liquid interaction parameter that correlates with α is the contact angle hysteresis (CAH) in the form [$\cos \theta_{rec} - \cos \theta_{adv}$], not any single contact angle value.[60, 61]

The wettability (or repellency) of a substrate can alternatively be viewed from a thermodynamic viewpoint that considers the free energies associated with the formation and elimination of interfacial areas. The equilibrium work of adhesion (W_e) is the reversible free energy associated with the creation and destruction of interfaces.[63] For the

case of liquid drops on solid surfaces, W_e can be calculated using the Young-Dupré equation:

$$W_e = \gamma_{LV}(1 + \cos \theta_e) \qquad (2)$$

where θ_e is the equilibrium (Young's) contact angle.[63-66] The solid-liquid interaction parameter that directly correlates with W_e is the dimensionless factor $[1 + \cos \theta_e]$. Many other terms are used in the literature to describe W_e, including "fundamental work of adhesion,"[67, 68] "thermodynamic work of adhesion,"[67] "basic work of adhesion,"[67] and, more generically, "work of adhesion."[30, 31, 66] The idealized Young-Dupré equation may not, in practice, describe typical processes. For instance, the forces required to remove Wilhelmy plates from liquids[63, 66] or to separate surfaces connected by a capillary bridge of water[69] are governed by the receding contact angle θ_{rec}. It was on the basis of this latter result[69] that Gao and McCarthy suggested[60, 61] that the work of adhesion could be quantified using:

$$W_p = \gamma_{LV}(1 + \cos \theta_{rec}) \qquad (3)$$

Here we will use Mittal's terminology[67] and refer to W_p as the "practical work of adhesion" because it involves the actual work required to separate a liquid from a surface. The solid-liquid interaction parameter that directly scales with W_p is the quantity $[1 + \cos \theta_{rec}]$ and, since $[1 + \cos \theta_{rec}]$ is always larger than $[1 + \cos \theta_e]$, W_p is always larger than W_e.

Ice adhesion strength may correlate more strongly with "water wettability" when "water wettability" is defined with respect to the shear and/or tensile processes described above. It is not obvious *a priori* which, if any, of the scaling relationships presented in Equations (1)-(3) should correlate with the strength of ice adhesion. All of these proposed

correlations require water contact angles to be reflective of ice-substrate interactions; the plausibility of this assumption will be later examined using our water contact angle and ice adhesion strength data. A correlation with $[\cos \theta_{rec} - \cos \theta_{adv}]$ may be reasonable if an interfacial liquid-like layer, which has been proposed for ice adhered to substrates,[20, 21, 70] promotes sliding of the interface prior to detachment of the ice column. It is also conceivable that ice adhesion strength scales with either W_e or W_p, as the adhesive detachment of ice from a substrate creates ice-vapor and substrate-vapor interfaces while destroying the ice-substrate interface.

Previously published data enable us to examine preliminarily the feasibility of these potential correlations. Murase and coworkers plotted the ice adhesion strength as a function of W_e for 22 different polymeric coatings.[30, 31] Generally the measured ice adhesion strengths were lower for samples with lower W_e, although significant scatter was present in the data; for example, ice adhesion strengths of 1000 kPa and 330 kPa were reported for samples with comparable W_e. Kulinich and Farzaneh reported an approximately linear correlation between average shear strength of ice adhesion and water CAH in the form CAH = $[\theta_{adv} - \theta_{rec}]$ for ten fluoropolymer/ nanopowder coatings.[53] The "water contact angles" (presumably advancing values) reported by Kulinich and Farzaneh for their samples only vary by ~13° and most of the differences in CAH between surfaces are, therefore, the result of variations in θ_{rec} due to water droplets being in either the fully wetted Wenzel[71] (low θ_{rec}) or the composite Cassie-Baxter[72] (high θ_{rec}) state.[53] Consequently, plots of the ice adhesion strength versus the scaling parameter $[1 + \cos \theta_{rec}]$ would also be approximately linear, consistent with a correlation between the ice adhesion strength and the practical work of adhesion of water W_p. Raraty

and Tabor[19] reported ice adhesion strengths and receding water contact angles on four different flat organic substrates. These ice adhesion strengths,[19] like those on surfaces studied by Kulinich and Farzaneh,[53] varied approximately linearly with the water dimensionless parameter $[1 + \cos \theta_{rec}]$, consistent with practical work of adhesion of water playing a key role in ice adhesion. While it is not possible to reach definitive conclusions given the limited amount of data reported in the literature, it does appear that ice adhesion strength correlates more strongly with either the roll-off angle for water drops or the practical work of adhesion of water than it does with static water contact angles.

In this work we examine the relationships between water wettability and ice adhesion strength on nominally smooth bare and coated steel discs. The Wenzel roughness for these surfaces (i.e., the actual surface area/ occluded surface area) is $r < 1.01$. Twenty-one different test coatings with a broad range of substrate-water interactions were employed, including commercially available polymers such as Tecnoflon® (a fluoroelastomer), poly(ethyl methacrylate) (PEMA), poly(methyl methacrylate) (PMMA), poly(butyl methacrylate) (PBMA), polycarbonate (PC), and crosslinked poly(dimethyl siloxane) (PDMS), as well as fluorodecyl polyhedral oligomeric silsesquioxane (fluorodecyl POSS) and blends of Tecnoflon® or PEMA with (1H,1H,2H,2H-heptadecafluorodecyl)$_8$Si$_8$O$_{12}$, or fluorodecyl POSS. Fluorodecyl POSS is a very low surface energy material ($\gamma_{SV} \approx 10$ mN/m)[73] that has been used to prepare a variety of water and oil repellent surfaces,[73-78] and solution blending provides a means of tuning the surface wettability of polymeric films/coatings cast from solution. For our samples, the average shear strength of ice adhesion varies nearly linearly with the

interaction parameter $[1 + \cos \theta_{rec}]$ that scales with the practical work of adhesion (W_p) for liquid water. This result suggests that maximizing the receding water contact angle θ_{rec} minimizes ice adhesion.

Experimental Section

Materials. Asahiklin (AK225, Asahi Glass Company) and dichloromethane (Aldrich) solvents were used as received. Tecnoflon[®] (Solvay Solexis), PEMA (Aldrich, M_w = 515 kg/mol), PMMA (Scientific Polymer Products, M_w = 540 kg/mol), PBMA (Aldrich, M_w = 337 kg/mol), and PC (Bayer) polymers were used as received. PDMS (Sylgard 184) was generously provided as a kit by Dow Corning; the base and curing agent were dissolved in Asahiklin in a 10:1 (by weight) ratio, spin-coated onto steel discs, and were heated for ~2 hrs at 60 °C to crosslink the chains. Fluorodecyl POSS was prepared following established protocols.[74] Steel discs were purchased from Marv-o-lus Manufacturing and were soaked in acetone and dried under an air purge prior to use. These discs are 25 mm in diameter, 1 mm thick, have a measured root-mean square roughness (R_q) = 1.0 ± 0.2 μm, and a measured Wenzel roughness (i.e., the actual surface area/ occluded surface area) $r < 1.01$ (see Figure S1 in the Supporting Information for a topographical depiction of a disc surface).

Coating Methodology. Solutions (total solids 20 mg/mL) were prepared by dissolving both the polymers and the fluorodecyl POSS in Asahiklin. Dichloromethane was used to prepare the PC solution because PC is not soluble in Asahiklin. Thin (~200-300 nm) coatings were deposited at room temperature on the steel discs via a spin coating

process; ~0.2 mL of solution was placed on top of each disc and the disc was spun at 900 rpm for 30 seconds.

Surface Characterization. The roughness of representative steel discs was measured using a Zygo interferometer. Scanning electron microscopy (SEM) images were acquired using a JEOL 6060 instrument operating at an acceleration voltage of 5 kV. Atomic force microscopy (AFM) measurements were carried out using a Veeco Metrology group, Dimension 3100 instrument operating in the tapping mode. X-ray photoelectron spectroscopy (XPS) was performed using a Kratos Axis Ultra X-ray photoelectron spectrometer manufactured by Kratos Analytical (Manchester, England). The monochromatized Al Kα source was operated at 15 kV and 10 mA (150 W) and emissions were collected at takeoff angles of 90° relative to the sample surface. Contact angles of deionized water (18 MΩ-cm, Millipore) on test surfaces were measured using a VCA2000 goniometer (AST Inc.). Advancing (θ_{adv}) and receding (θ_{rec}) angles were measured as water was supplied via a syringe into or out of sessile droplets (drop volume ~5 μL).

Ice Adhesion Measurements. While goniometers are widely used to measure liquid contact angles, there are no analogous, readily available commercial instruments designed to measure solid-solid (e.g., ice-substrate) adhesion strengths. A few groups have deposited glaze ice by spraying super-cooled water droplets over test substrates and then measured the average shear strength of ice adhesion using a centrifuge apparatus.[51-55, 57, 58] Although this setup is designed to mimic the environmental icing conditions encountered by, for example, power lines subject to freezing rain or airplanes colliding with supercooled water droplets in the atmosphere, it is not practical for most

academic laboratories because it requires an icing chamber and complex centrifuge set-up. A number of other groups have used simpler apparatus that involve pouring liquid water onto a test substrate, freezing the water, and then measuring the average shear stress required to remove the ice from the test surface.[12, 19, 23-25, 27, 30, 31, 34, 35, 43] We designed and constructed an adhesion test apparatus broadly following the physical principles of this latter strategy. Water columns were frozen to coated steel discs using the protocol summarized schematically in Figure 1 and described below. Coated steel discs were first clamped to a custom-built base plate (4 x 5 array). Deionized water (1.5 mL) was syringed into 20 glass cuvettes (1 cm x 1 cm x 4.4 cm, Scientific Equipment of Houston) that had been modified by: (1) polishing the tops of the open ends using a Buehler EcoMet 250/300 Grinder-Polisher equipped with 1200 grit; (2) treating the cuvettes with 1H,1H,2H,2H-perfluorodecyltrichlorosilane (Gelest) vapor to reduce their surface energies. These modified cuvettes were then loaded into a custom-built sample holder (4 x 5 array). The base plate was inverted and placed on top of the sample holder, and this assembly was bolted together to provide flush contact between the cuvettes and test substrates. Water typically did not leak from the inverted cuvettes provided the glass had been polished to enhance the physical contact with the test substrate and treated with 1H,1H,2H,2H-perfluorodecyltrichlorosilane to reduce its surface energy and water wettability. This assembly was mounted on top of a liquid-cooled Peltier cooling plate (TECA Corporation, model LHP-800CP) that was housed in a low-humidity nitrogen atmosphere to minimize frost formation on the samples and test apparatus. The temperature of the cooling plate surface was monitored using a thermocouple washer bolted to the top of the plate, and the target temperature was typically −10 °C to facilitate

10

comparison with previously reported data.[51, 52]) The water was frozen overnight (~10 –

15 hours) and the sample holder was carefully removed from the assembly, leaving ice

columns encased in cuvettes and adhered to the test substrates. The force required to

detach each ice column from its test substrate was measured by propelling the 0.8 cm

diameter probe of a force transducer (Imada, model ZP–44) into the side of the cuvette at

a constant velocity of 0.5 mm/s unless otherwise specified. The probe velocity was

controlled using a motion stage (MICOS, model VT80). The probe was located less than

2 mm above the substrate surface to minimize torque on the ice sample. The measured

maximum force at break was converted into shear strength of ice adhesion by dividing by

the known cross-sectional area (1 cm^2) of the ice-substrate interface. A photograph of the

assembled apparatus in operation is provided in Figure S2 in the Supporting Information.
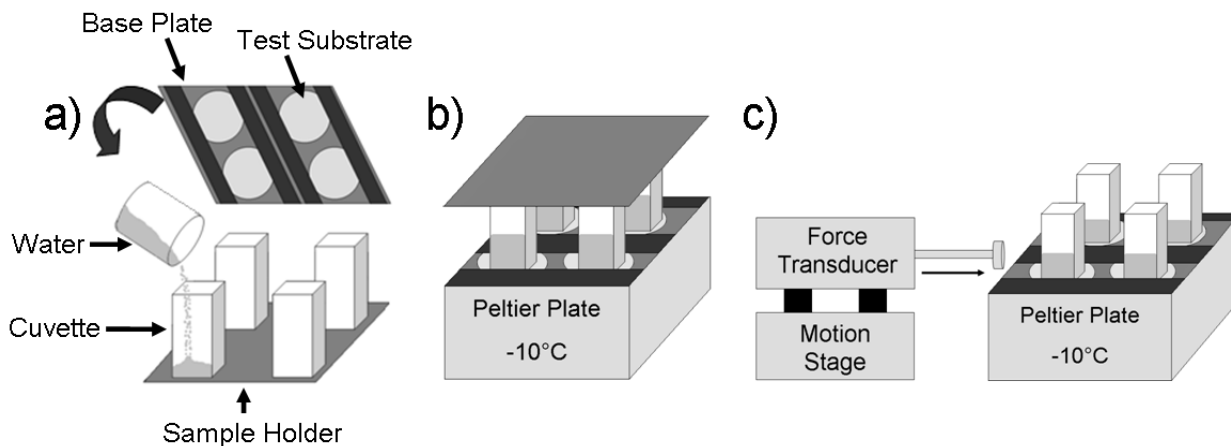
Figure 1. Schematic depiction of the procedure used to freeze water columns on test substrates and to measure the ice adhesion strength. The actual apparatus can hold a 4 x 5 array of samples; a 2 x 2 array is used here for ease of illustration. a) Deionized water is poured into cuvettes housed in a sample holder (bottom) and coated steel discs are clamped onto a base plate (top). The samples attached to the base plate are then mounted flush against the tops of the cuvettes. b) The base plate-sample holder assembly is taken into a glove box operating under a nitrogen atmosphere, inverted, and bolted to a Peltier cooling plate whose surface is thermostated at a target temperature (–10 °C unless otherwise specified). An insulating foam box is placed over the assembly to reduce the cooling load required of the chiller and the water columns are allowed to freeze for 10–15 hours. c) The top sample holder is removed and the probe of a force transducer is propelled at 0.5 mm/s, unless otherwise specified, into the side of each cuvette until the ice detaches from the test surface. The maximum force is recorded and converted into shear strength of ice adhesion using the known cross-sectional area of the ice-substrate interface.

Results and Discussion

Water contact angle and ice adhesion measurements (–10 °C, 0.5 mm/s probe velocity) for the 22 tested surfaces are summarized in Table 1. Notably, the magnitudes of the measured ice adhesion strengths (165-510 kPa) are comparable to those reported in the literature for textured surfaces using a centrifuge set-up (50-500 kPa),[51-55] evidence that the apparatus described in Figure 1 yields quantitatively meaningful data. Each test coating was applied to at least four different steel discs, one of which was a control that was not subjected to icing conditions. Water contact angles were measured before and after each ice adhesion measurement to probe the durability of the coatings. Contact

angles measured on the tested substrates were within the experimental uncertainties of those measured on the control surfaces, indicating the (typically 3-5) ice adhesion tests did not damage or remove the deposited coatings. Generally the removal of ice from test surfaces was adhesive in nature, with no residual ice visible on the coating following testing. In some cases, however, mixed-mode[67] failure was observed, with some shards of ice (< 25% of the ice-substrate interfacial area) remaining adhered to the test substrate following detachment of the macroscopic ice column. The probability of a mixed-mode failure generally increased as the receding water contact angle θ_{rec} decreased, as can be seen upon examination of the fractions of tests with completely adhesive failure (i.e., no ice shards remaining on the substrate) that are provided in Table 1. The measured ice adhesion strengths did not significantly vary for these two failure modes, and data from both subpopulations are included in the average shear strength of ice adhesion values reported in Table 1.

Table 1. Measured Water Contact Angles and Average Shear Strengths of Ice Adhesion for the

22 Tested Surfaces

Substrate	θ_{adv}, water[a]	θ_{rec}, water[a]	# of Ice Adhesion Tests	Fraction of Tests with Completely Adhesive Failure[b]	Average Shear Strength of Ice Adhesion at −10 °C (kPa)[c]
Bare Steel	86.2 ± 3.3	25.8 ± 2.5	9	0.33	698 ± 112
PMMA	83.6 ± 3.6	60.7 ± 1.3	11	0.73	463 ± 65
PC	93.4 ± 1.0	73.9 ± 3.3	7	0.86	400 ± 83
PBMA	92.8 ± 2.4	74.6 ± 1.7	9	0.44	384 ± 52
PDMS (Sylgard 184)	108.9 ± 1.5	91.7 ± 5.1	9	1.00	291 ± 44
PEMA	84.6 ± 2.4	68.0 ± 2.5	9	0.67	510 ± 101
99/1 PEMA/ fluorodecyl POSS	97.5 ± 2.2	67.5 ± 2.2	9	0.22	475 ± 50
97/3 PEMA/ fluorodecyl POSS	105.4 ± 3.7	77.0 ± 4.7	8	1.00	367 ± 86
95/5 PEMA/ fluorodecyl POSS	122.2 ± 2.0	104.0 ± 5.3	8	1.00	278 ± 93
90/10 PEMA/ fluorodecyl POSS	122.6 ± 2.1	107.6 ± 6.9	12	0.92	247 ± 45
80/20 PEMA/ fluorodecyl POSS	123.8 ± 1.2	118.2 ± 2.4	7	1.00	165 ± 27
70/30 PEMA/ fluorodecyl POSS	124.2 ± 0.9	116.4 ± 2.9	9	1.00	166 ± 44
50/50 PEMA/ fluorodecyl POSS	125.0 ± 1.7	114.1 ± 2.4	8	1.00	185 ± 57
Tecnoflon	118.3 ± 1.4	73.7 ± 2.1	17	0.76	389 ± 63
99/1 Tecnoflon/ fluorodecyl POSS	125.7 ± 1.9	79.2 ± 3.4	13	0.92	392 ± 88
97/3 Tecnoflon/ fluorodecyl POSS	127.0 ± 1.7	87.7 ± 4.8	11	0.82	412 ± 64
95/5 Tecnoflon/ fluorodecyl POSS	126.6 ± 1.2	92.9 ± 4.3	15	1.00	328 ± 97
90/10 Tecnoflon/ fluorodecyl POSS	126.6 ± 0.8	98.0 ± 5.3	9	1.00	345 ± 104
80/20 Tecnoflon/ fluorodecyl POSS	126.0 ± 0.9	103.7 ± 4.3	11	1.00	313 ± 70
70/30 Tecnoflon/ fluorodecyl POSS	125.2 ± 0.8	110.0 ± 3.1	9	1.00	205 ± 40
50/50 Tecnoflon/ fluorodecyl POSS	128.3 ± 1.1	108.7 ± 3.4	8	1.00	265 ± 42
Fluorodecyl POSS	137.6 ± 4.8	110.0 ± 3.8	15	1.00	250 ± 54

[a] Uncertainties are standard deviations in all data collected before and after ice adhesion tests. [b] Mixed-mode[67] failures with small shards of ice remaining adhered to test substrates were observed for some samples. [c] The force probe impacted the cuvette-encased ice columns at a velocity of 0.5 mm/s, and uncertainties are computed using a Student's t-test with 95% confidence intervals.

The measured average shear strengths of ice adhesion are plotted against two different water contact angles in Figure 2 to allow for ready comparison with previous literature.[23-25, 31, 34, 42, 43, 51, 53] It is difficult to measure equilibrium static water contact angles because droplets can adopt long-lived metastable configurations with an instantaneous contact angle anywhere between θ_{adv} and θ_{rec}.[61, 79] As an alternative, two values were chosen that are believed to provide plausible bounds for the equilibrium contact angle. The advancing contact angle θ_{adv}, which some have used as an approximation of θ_e,[80] is used as the abscissa in Figure 2a. Other groups have suggested that equilibrium-like contact angles can be obtained by vibrating liquid drops.[80-82] All of these vibrated drops, regardless of initial position, consistently adopted a final configuration with a unique contact angle between θ_{adv} and θ_{rec}. This angle $\bar{\theta}_e$ can be estimated[80-82] from θ_{adv} and θ_{rec} measurements using:

$$\cos \bar{\theta}_e = 0.5 \, (\cos \theta_{adv} + \cos \theta_{rec}) \tag{4}$$

Measurements of the advancing and receding contact angles θ_{adv} and θ_{rec} are reproducible,[61] enabling consistent estimation of $\bar{\theta}_e$. Static contact angles measured using typical goniometric techniques are reportedly[80] higher than $\bar{\theta}_e$, leading to the selection of $\bar{\theta}_e$ as a lower bound for single water contact angle measurements and as the abscissa in Figure 2b. The curves in Figure 2a and Figure 2b both generally have a negative slope, consistent with some literature reports that ice adhesion decreases with increasing water contact angle.[34, 42, 43, 51] There is less scatter present when $\bar{\theta}_e$ is used as the abscissa (for a linear fit, the square of the correlation coefficient (R^2) = 0.82) than when θ_{adv} (for a linear fit, $R^2 = 0.54$) is selected.
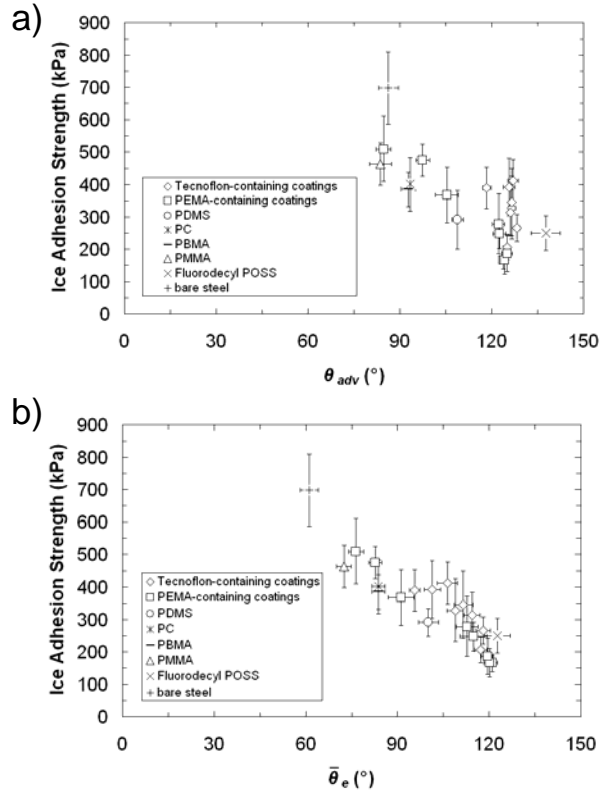
Figure 2. Average shear strengths of ice adhesion measured at −10 °C for bare steel and 21 different coatings and plotted against two different measured water contact angles; (a) the advancing water contact angle θ_{adv} and (b) the estimated equilibrium contact angle $\bar{\theta}_e$ computed using the proposed[59, 80-82] approximation given in Equation (4). Static water contact angles reported in the literature likely fall between θ_{adv} and $\bar{\theta}_e$,[80] and these plots facilitate comparison with previous presentations of ice adhesion measurements.[23-25, 31, 34, 42, 43, 51, 53]

The concepts of shear and tensile wettability (Equations (1)-(3)), which require measurements of θ_{adv} and θ_{rec}, can be used to describe solid-liquid interactions more accurately and completely than any single contact angle value.[60, 61] Our data can be used to test the applicability of this wettability framework to substrate-ice adhesion. We begin our examination of the applicability of the shear and tensile adhesion framework for water to ice-substrate adhesion strengths with a comparison of the ice adhesion strength and the water CAH parameter [cos θ_{rec} − cos θ_{adv}] that scales with liquid drop roll-off (see

Equation (1)). This interaction parameter could plausibly influence ice adhesion strength

if the interface between ice and a substrate is comprised of a liquid-like layer, as has been

proposed;[20, 21, 70] such a liquid-like interface could facilitate lateral sliding prior to

detachment of the ice column. The measured ice adhesion strengths are plotted in

Figure 3 against the CAH parameter [$\cos \theta_{rec} - \cos \theta_{adv}$], which scales with liquid drop

roll-off angle (see Equation (1)). Data acquired from test substrates with $\theta_{adv} > 105°$

correlate almost linearly ($R^2 = 0.86$) with [$\cos \theta_{rec} - \cos \theta_{adv}$], a result consistent with

Kulinich and Farzaneh's measurements of the strength of ice adhesion to rough

fluoropolymer/ nanopowder coatings.[53] Kulinich and Farzaneh used CAH = [$\theta_{adv} - \theta_{rec}$] as

the abscissa, while we are utilizing the [$\cos \theta_{rec} - \cos \theta_{adv}$] scaling parameter that appears

in Equation (1). The differences in the plot shapes are relatively minor for our data, as

can be seen from a comparison of Figure 3 and Figure S3 in the Supporting Information.

Notably, and unlike that of Kulinich and Farzaneh,[53] our data set contains numerous

points that deviate significantly from this nearly linear trend. The six samples with

$\theta_{adv} < 100°$ adhere to ice more strongly than anticipated based upon the linear best fit of

the ice adhesion strength versus [$\cos \theta_{rec} - \cos \theta_{adv}$], providing compelling evidence that

ice adhesion strength does not always correlate linearly with water CAH. Further

evidence that [$\cos \theta_{rec} - \cos \theta_{adv}$] is not the proper scaling factor for ice adhesion strength

comes from extrapolations of the linear fits to both our and Kulinich and Farzaneh's

data.[53] In neither case does a plausible linear fit pass through the origin, suggesting that

even as [$\cos \theta_{rec} - \cos \theta_{adv}$] $\rightarrow 0$, ice will still adhere to substrates; presumably the

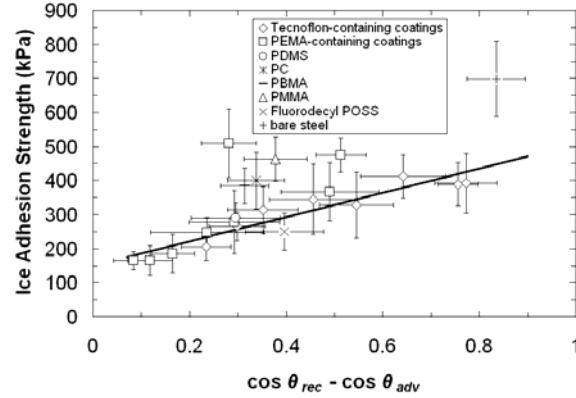strength of ice adhesion will approach zero when the correct correlation analysis is
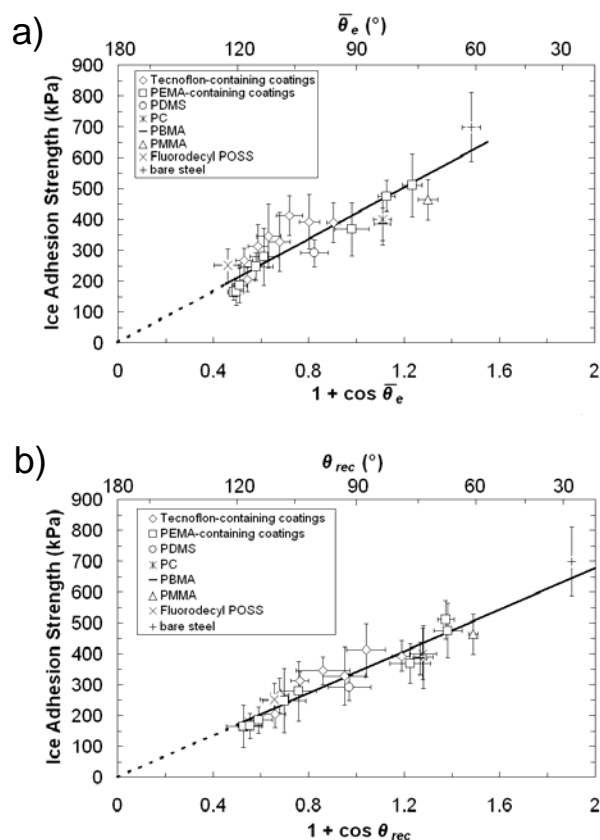
applied.

Figure 3. Average shear strengths of ice adhesion measured at −10 °C for bare steel and 21 different coatings plotted against a measure of water contact angle hysteresis which scales with liquid drop roll-off angle (see Equation (1)). The solid line is the linear best fit to the data acquired from the 16 surfaces with $\theta_{adv} > 105°$.

Ice adhesion strength is next considered in the context of tensile phenomena for liquid water. Average shear strengths of ice adhesion are presented in Figure 4 as functions of parameters that scale with the equilibrium $(1 + \cos \overline{\theta}_e$, Figure 4a) and practical $(1 + \cos \theta_{rec}$, Figure 4b) works of adhesion for water on these same surfaces. We believe that the average shear strength of ice adhesion should approach zero along with the governing interaction parameter, and, consequently, the data were fit with the constraint that the linear correlations pass through the origin. The solid/dashed lines depicted in Figure 4 are these best fits (with the dashed portions representing the extrapolation to the origin). The best fit correlation ($R^2 = 0.92$, Figure 4b) between ice adhesion strength and $[1 + \cos \theta_{rec}]$ yields the following expression for the average shear strength of ice adhesion:

$$\tau_{ice} = (340 \pm 40 \text{ kPa})(1 + \cos \theta_{rec}) \tag{5}$$

18

This correlation is significantly stronger than the correlation with $[1 + \cos \bar{\theta}_e]$ ($R^2 = 0.80$,

Figure 4a). The linearity of the data depicted in Figure 4b is consistent with the earlier

assumption that water contact angles are reflective of ice-substrate interactions.

Furthermore, the correlation with $[1 + \cos \theta_{rec}]$ improves only slightly (R^2 increases by

< 0.001) when the linear best fit is not required to pass through the origin, supporting the

hypothesis that the average shear strength of ice adhesion should approach zero along

with the correct scaling parameter. This correlation with $[1 + \cos \theta_{rec}]$ is also stronger

than Murase et al.'s proposed relationship between the ice adhesion strength and the work

of adhesion for water computed using Bangham and Razouk's modification[83] of

Equation (2) that incorporates a reduction in solid surface energy due to adsorption of

water vapor.[30, 31]

Figure 4. Average shear strengths of ice adhesion measured at −10 °C for bare steel and 21 different coatings plotted against water contact angle parameters that scale with (a) the equilibrium work of adhesion for liquid water (see Equation (2)) and (b) the practical work of adhesion for liquid water (see Equation (3)). The straight lines are the linear best fits that pass through each origin, with the solid portions of the lines encompassing the measured data and the dashed portions representing the extrapolation to the origin. The linear fit for (b) ($\tau_{ice} = (340 \pm 40$ kPa$)(1 + \cos \theta_{rec})$, $R^2 = 0.92$) is significantly better than that for (a) ($R^2 = 0.80$).

The validity of the proposed scaling between ice adhesion strength and

$[1 + \cos \theta_{rec}]$ is further supported by Kulinich and Farzaneh's data,[53] which are re-plotted

against $[1 + \cos \theta_{rec}]$ in Figure S4 in the Supporting Information. For this plot, receding

water contact angles θ_{rec} were calculated using the reported CAH and the assumption that

the "water contact angles" listed in the paper[53] were advancing values. The scaling

argument that the ice adhesion strength should be zero when the practical work of

adhesion for water is zero was again used to require the linear best fit to pass through the

origin. The high correlation coefficient for this linear best fit of the Kulinich and

Farzaneh data[53] ($R^2 = 0.93$, see Figure S4) is further support for our proposal that the

measured shear strength of ice adhesion depends on the magnitude of the liquid water

parameter [1 + cos θ_{rec}] which is measured on the solid surface under consideration.

The sensitivities of the measured average shear strengths of ice adhesion to

variations in temperature and the speed of the incident force transducer were probed for

four test substrates that span a broad range of receding water contact angle values:

80/20 PEMA/ fluorodecyl POSS (θ_{rec} = 118.2° ± 2.4°), 90/10 PEMA/ fluorodecyl POSS

(θ_{rec} = 107.6° ± 6.9°), PDMS (Sylgard 184) (θ_{rec} = 91.7° ± 5.1°), and PBMA

(θ_{rec} = 74.6° ± 1.7°). These experimental results are summarized in Table 2 and in Figure

S7 in the Supporting Information. The values of the average shear strength of ice

adhesion for each set of test conditions were plotted against [1 + cos θ_{rec}] and linear best

fits through each origin were obtained and are reported in Table 3. These linear fits

depend on data from all four test substrates and provide a quantitative means of

comparing the ensembles of data collected at the five different test conditions. The slopes

of the fits to the data acquired at various probe displacement speeds at −10 °C are clearly

not statistically different, indicating that the shear stress of ice detachment is not sensitive

to the incident probe speed over this 0.1 mm/s – 1.5 mm/s range. Although the best fit

slope of the −5 °C data is larger than those obtained by fitting the −10 °C and −15 °C data,

statistical analysis using Student's t-test reveals that there is only a 45% chance that the

highest and lowest slopes of the fits (obtained from the −5 °C and −15 °C data) are in fact

different, too small of a probability to draw any firm conclusions. Raraty and Tabor[19] and

Landy and Freiberger[24] similarly reported that ice adhesion strength is not sensitive to

substrate temperature over this –5 °C to –15 °C range provided the interfacial failure is

adhesive.

Table 2. Measured Receding Water Contact Angles and Average Shear Strengths of Ice

Adhesion for Four Test Substrates at Several Temperatures and Force Transducer Speeds

Substrate Coating	Temperature (°C)	Incident Probe Speed (mm/s)	θ_{rec}, water[a]	# of Ice Adhesion Tests	Fraction of Tests with Completely Adhesive Failure[b]	Average Shear Strength of Ice Adhesion at –10 °C (kPa)[c]
80/20 PEMA/ fluorodecyl POSS	–10 °C	0.1	118.2 ± 2.4	10	1.00	196 ± 38
	–10 °C	0.5		7	1.00	165 ± 27
	–10 °C	1.5		10	1.00	196 ± 35
	–5 °C	0.5		8	1.00	215 ± 21
	–15 °C	0.5		10	0.90	160 ± 46
90/10 PEMA/ fluorodecyl POSS	–10 °C	0.1	107.6 ± 6.9	8	1.00	227 ± 54
	–10 °C	0.5		12	0.92	247 ± 45
	–10 °C	1.5		10	1.00	234 ± 59
	–5 °C	0.5		8	1.00	297 ± 47
	–15 °C	0.5		8	1.00	220 ± 52
PDMS (Sylgard 184)	–10 °C	0.1	91.7 ± 5.1	8	1.00	264 ± 26
	–10 °C	0.5		9	1.00	291 ± 44
	–10 °C	1.5		7	1.00	269 ± 111
	–5 °C	0.5		8	0.88	328 ± 91
	–15 °C	0.5		6	1.00	279 ± 56
PBMA	–10 °C	0.1	74.6 ± 1.7	8	0.75	413 ± 98
	–10 °C	0.5		9	0.44	384 ± 52
	–10 °C	1.5		8	0.50	428 ± 93
	–5 °C	0.5		7	0.63	485 ± 133
	–15 °C	0.5		9	0.22	400 ± 98

[a] Uncertainties are standard deviations in all of the data collected before and after ice adhesion tests. [b] Mixed-mode[67] failures with small shards of ice remaining adhered to test substrates were observed for some samples. [c] The uncertainties were calculated using a Student's t-test with 95% confidence intervals.

Table 3. Linear Best Fits of Plots of Average Shear Strength of Ice Adhesion versus Receding Water Contact Angles at Several Temperatures and Incident Force Transducer Speeds

Test Condition	Temperature (°C)	Incident Probe Speed (mm/s)	Number of Test Substrates	Slope of Linear Best Fit[a] (kPa)	R^2 of Linear Best Fit
1	−10 °C	0.1	4	314 ± 133	0.90
2	−10 °C	0.5	22[b]	340 ± 40	0.92
2	−10 °C	0.5	4[c]	311 ± 84	0.95
3	−10 °C	1.5	4	323 ± 109	0.90
4	−5 °C	0.5	4	378 ± 125	0.92
5	−15 °C	0.5	4	307 ± 101	0.98

[a] Uncertainties were computed using a Student's t-test with 95% confidence intervals.
[b] Data from all 22 test substrates listed in Table 1 are used to calculate the fit. [c] Only data from 80/20 PEMA/ fluorodecyl POSS, 90/10 PEMA/ fluorodecyl POSS, PDMS (Sylgard 184), and PBMA test samples were used to compute the fit.

While it is clearly economically desirable to minimize the amount of relatively expensive fluorodecyl POSS incorporated into coatings, examination of the data reported in Table 1 suggests that there are also performance benefits associated with "diluting" the fluorodecyl POSS with commercially available polymers. Water has the highest advancing angle θ_{adv} on pure fluorodecyl POSS, but does not exhibit the highest receding angle θ_{rec} on this fluorinated coating and, consequently, ice adheres to discs coated with pure fluorodecyl POSS ($\theta_{rec} = 110.0 \pm 3.8°$, $\tau_{ice} = 250 \pm 54$ kPa) more strongly than it does to discs coated with, for example, 80/20 PEMA/ fluorodecyl POSS ($\theta_{rec} = 118.2 \pm 2.4°$, $\tau_{ice} = 165 \pm 27$ kPa). The 80/20 PEMA/POSS surface was selected for comparison because of its combination of a low fluorodecyl POSS loading and a minimal adherence to ice. The relative water repellency and "icephobicity" of coatings are connected to the topographic structure of the surface of the deposited film. SEM and

tapping-mode AFM were used to probe surface topographies of ~200-300 nm thick layers of pure fluorodecyl POSS and 80/20 PEMA/ fluorodecyl POSS that were deposited on silicon wafers by spin coating. The pure fluorodecyl POSS coatings are substantially rougher than the 80/20 PEMA/ fluorodecyl POSS films in the SEM images presented in Figure S8. This observation was confirmed by AFM height measurements presented in Figure S9 that yielded a root-mean square roughness R_q = 39 nm and a Wenzel roughness r = 1.74 for pure fluorodecyl POSS, and R_q = 2 nm and r = 1.04 for the 80/20 PEMA/POSS coating. We believe that the increased roughness of the pure fluorodecyl POSS coating resulting from the spin-coating process leads to a reduction in θ_{rec}[63] and the concomitant increase in ice adhesion strength compared to the smoother 80/20 PEMA/ fluorodecyl POSS surface. Blending PEMA with fluorodecyl POSS is thus not only economically desirable but also improves coating performance by (i) facilitating the deposition of a smooth film with high fluorine content that exhibits maximum values of receding contact angles; (ii) possibly enhancing mechanical properties by incorporating a durable polymer binder into the coating.

The molecular and topographic structure of the 80/20 PEMA/fluorodecyl POSS film deposited on silicon were further probed using XPS and AFM phase imaging. Atomic ratios computed using the XPS survey spectra are 1.54 for F/C, 0.11 for O/C, and 0.09 for Si/C. These values are close to those expected for pure fluorodecyl POSS (1.7 for F/C, 0.15 for O/C, and 0.1 for Si/C),[77] indicative of a thermodynamically driven segregation or "blooming"[75] of the fluorodecyl POSS towards the surface. Additional information about the molecular composition of the surface can be gleaned from XPS by examining the high-resolution carbon 1s spectrum that is presented in Figure 5a. The

peaks in this spectrum were indexed by comparing the measured binding energies at peak maxima with standard spectra available for PEMA and poly(vinylidene fluoride).[84] The peak associated with the $-CF_2-$ moiety is roughly four times as intense as that associated with the $-CH_2-$ moiety, further evidence that fluorodecyl POSS (which is the sole contributor to the $-CF_2-$ peak) has a significant surface presence. The tapping-mode AFM phase image presented in Figure 5b is also consistent with this XPS analysis. The bright regions in this micrograph represent fluorodecyl POSS aggregates that have bloomed to the surface during the spin coating and solvent evaporation process.[75] Presumably these fluorodecyl POSS aggregates strongly reduce liquid water wettability and are responsible for the relatively icephobic characteristics of the 80/20 PEMA/ fluorodecyl POSS surface.
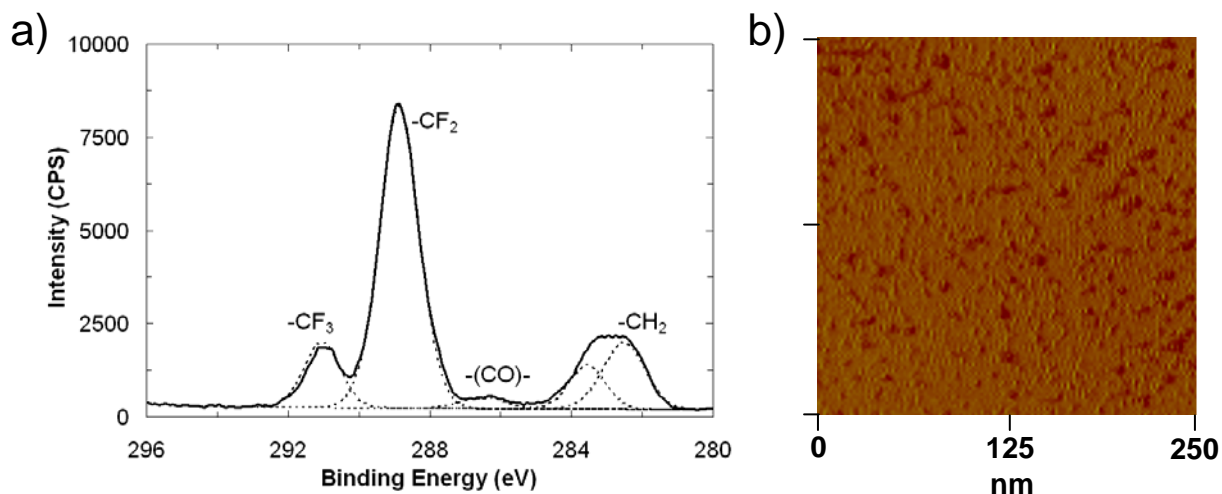

Figure 5. Surface characterization of a ~200-300 nm thick layer of 80/20 PEMA/ fluorodecyl POSS spin-coated onto a silicon wafer. a) High-resolution carbon 1s X-ray photoelectron spectrum. Peaks corresponding to various carbon moieties located near the surface are labeled. b) Phase image of a 250 nm x 250 nm section of the film surface acquired using tapping-mode AFM. The phase angle scale on the image is 0° to 8°.

We believe this 80/20 PEMA/ fluorodecyl POSS coating with $\theta_{rec} = 118.2° \pm 2.4°$ (and the other fluorodecyl-POSS containing surfaces with similar values of θ_{rec}) essentially yields the minimum strength of ice adhesion that is attainable by reducing the water wettability of smooth surfaces. It is possible that other attributes of the coatings, such as their viscoelastic properties,[27, 30, 31] also influence ice adhesion strength, although the strong correlation presented in Figure 4b implies that these effects are secondary compared to the receding water contact angle parameter [$1 + \cos \theta_{rec}$], at least for the coatings investigated here. The fit to our data provided in Equation (5) suggests that a further appreciable reduction in [$1 + \cos \theta_{rec}$] and thus ice adhesion could only be attained by significantly increasing the receding water contact angle above $\theta_{rec} \sim 120°$. However, the maximum receding water contact angle attainable on a smooth surface with known materials chemistry is $\theta_{rec} \sim 120°$.[75, 85] Given this current upper bound in θ_{rec}, it is more likely that further significant reductions in ice adhesion strength will be brought about by incorporating microscale and/or nanoscale texture into surfaces. Effective icephobic surfaces will likely allow water droplets to freeze while in the composite (Cassie-Baxter) state, with a reduction in the substrate-ice interfacial area (and possibly the ice adhesion strength) because of the air trapped beneath the ice. The quantitative data recently reported by Kulinich and Farzaneh[53] and Dotan et al.[51] on textured surfaces can be used to evaluate the validity of this prediction. The low shear stresses of ice detachment reported by these groups were attributed to water droplets freezing in the composite state.[51, 53] (A few other groups also investigated ice adhesion on textured surfaces, but did not report the ice adhesion strengths and/or θ_{rec} values needed for inclusion in the compilation.[50, 52, 55-58]) The Kulinich and Farzaneh[53] and Dotan et al.[51] data are plotted

26

along with both our data and the best fit to our data in Figure 6. Given that measured values of the shear strengths of adhesion may generally be sensitive to the specific details of test configurations and conditions,[67] the reported data are in good quantitative agreement with the predicted correlation provided in Equation (5). Additional efforts aimed at preparing micro- and nanotextured icephobic surfaces with very large receding water contact angles are currently underway in our laboratory.
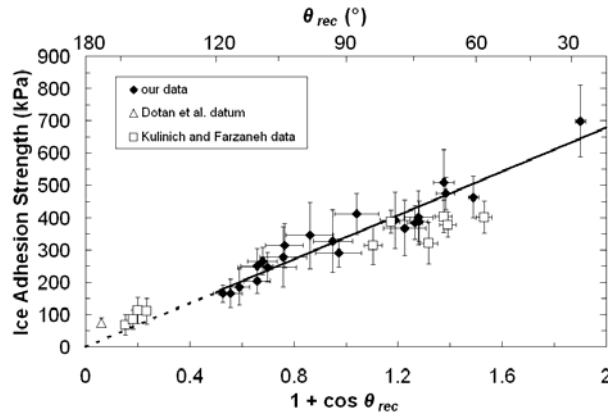

Figure 6. Compilation of average shear strengths of ice adhesion measured in this work (22 nominally smooth test substrates at −10 °C, ◆), by Kulinich and Farzaneh[53] (10 textured test substrates at −10 °C, □), and by Dotan et al.[51] (one textured test substrate at −8 °C, Δ). The solid and dashed lines represent the linear best fit to our data (predicted average shear strength of ice adhesion $\tau_{ice} = (340 \pm 40 \text{ kPa})(1 + \cos \theta_{rec})$, $R^2 = 0.92$).

Conclusions

The average shear strengths of ice adhesion were measured on bare steel discs and discs coated with twenty-one different materials with a range of liquid water wettabilities. These measured ice adhesion strengths were compared to different goniometric measures of water wettability that can be used to describe the interactions of the substrates with liquid water and that scale respectively with liquid drop roll-off ($[\cos \theta_{rec} - \cos \theta_{adv}]$, Equation (1)), equilibrium work of adhesion ($[1 + \cos \bar{\theta}_e]$, Equation (2)), and practical

work of adhesion ($[1 + \cos \theta_{rec}]$, Equation (3)).[60, 61] A strong correlation was found between our measurements of the average shear strength of ice adhesion and the liquid water practical work of adhesion scaling parameter $[1 + \cos \theta_{rec}]$, suggesting that the "icephobicity" of nominally smooth surfaces can be predicted simply by measuring the receding contact angle for water droplets on the substrate (see Equation (5)). We believe that the fluorodecyl POSS-containing coatings described here have nearly reached the attainable limit of icephobicity for smooth surfaces, as no known materials have receding water contact angles that are significantly above the $\theta_{rec} = 118.2° \pm 2.4°$ measured on the 80/20 PEMA/ fluorodecyl POSS coating.[75, 85] Further reductions in ice adhesion strengths will therefore likely require manipulation of surface texture (e.g., micro- and nano-textures and/or hybrid hydrophilic/hydrophobic surfaces[86]) to enable incident water drops to freeze in the composite (Cassie-Baxter) state.

References

(1) Civil Aviation Authority. *Aircraft Icing Handbook*, 2000.
(2) Sayward, J. M. *Special Rep. 79-11*, U.S. Army Cold Regions Research and
    Engineering Laboratory, Hanover, NH, 1979.
(3) Boluk, Y. *Transports Canada Publication TP 12860E*. Quebec, Canada, 1996.
(4) Dutta, P. K.; Ryerson, C. C.; Pergantis, C. *Mater. Res. Soc. Symp. Proc.* **2005***, 851*,
    563-574.
(5) Landy, M.; Freiberger, A. *Nav. Eng. J.* **1968***, 80*, 63-72.
(6) Ryerson, C. C. *Cold Reg. Sci. Technol.* **2010** *In Press*.
(7) Laforte, J. L.; Allaire, M. A.; Laflamme, J. *Atmos. Res.* **1998***, 46*, 143-158.
(8) Dalili, N.; Edrisy, A.; Carriveau, R. *Renewable & Sustainable Energy Reviews* **2009***,
    13*, 428-438.
(9) Parent, O.; Ilinca, A. *Cold Reg. Sci. Technol.* **2010***, In Press*.
(10) Frankenstein, S.; Tuthill, A. M. *J. Cold Regions Eng.* **2002***, 16*, 83-96.
(11) Saito, H.; Takai, K.; Takazawa, H.; Yamauchi, G. *Mater. Sci. Res. Int.* **1997***, 3*, 216-
    219.
(12) Saito, H.; Takai, K.; Yamauchi, G. *Mater. Sci. Res. Int.* **1997***, 3*, 185-189.
(13) Air Force Fact Sheet Update. *The Role of Deicing and Anti-icing in the Air Force*,
    1998.
(14) United States Environmental Protection Agency. *Storm Water Technology Fact
    Sheet: Airplane Deicing Fluid Recovery Systems*; EPA 832-F-99-043, 1999.
(15) Baker, H. R.; Bascom, W. D.; Singleterry, C. R. *J. Colloid Sci.* **1962***, 17*, 477-491.
(16) Ford, T. F.; Nichols, O. D. *Naval Research Lab. Report 5832*, 1962.
(17) Ayres, J.; Simendinger, W. H.; Balik, C. M. *J. Coat. Technol. Res.* **2007***, 4*, 463-471.
(18) Ayres, J.; Simendinger, W. H.; Balik, C. M. *J. Coat. Technol. Res.* **2007***, 4*, 473-481.
(19) Raraty, L. E.; Tabor, D. *Proc. Roy. Soc.* **1958***, A245*, 184-201.
(20) Jellinek, H. H. G. *J. Colloid Sci.* **1959***, 14*, 268-280.
(21) Jellinek, H. H. *Can. J. Phys.* **1962***, 40*, 1294-1309.
(22) Stallabrass, J. R.; Price, R. D. *Can. Aeronaut. Space J.* **1963***, 9*, 199-199-204.
(23) Bascom, W. D.; Cottington, R. L.; Singleterry, C. R. *Naval Research Lab. Report
    6350*, 1966.
(24) Landy, M.; Freiberger, A. *J. Colloid Interface Sci.* **1967***, 25*, 231-244.
(25) Bascom, W. D.; Cottington, R. L.; Singleterry, C. R. *J. Adhesion* **1969**, 246-263.
(26) Jones, J. R.; Gardos, M. N. *Lubrication Engineering* **1972***, 28*, 464-471.
(27) Jellinek, H. H. G.; Kachi, H.; Kittaka, S.; Lee, M.; Yokota, R. *Colloid Polym. Sci.*
    1978*, 256*, 544-551.
(28) Andrews, E. H.; Lockington, N. A. *J. Mater. Sci.* **1983***, 18*, 1455-1465.
(29) Andrews, E. H.; Majid, H. A.; Lockington, N. A. *J. Mater. Sci.* **1984***, 19*, 73-81.
(30) Murase, H.; Nanishi, K. *Ann. Glaciol.* **1985***, 6*, 146-149.

(31) Murase, H.; Nanishi, K.; Kogure, H.; Fujibayashi, T.; Tamura, K.; Haruta, N. *J. Appl. Polym. Sci.* **1994**, *54*, 2051-2062.

(32) Sonwalkar, N.; Sunder, S. S.; Sharma, S. K. *J. Raman Spectrosc.* **1991**, *22*, 551-557.

(33) Sonwalkar, N.; Sunder, S. S.; Sharma, S. K. *Appl. Spectrosc.* **1993**, *47*, 1585-1593.

(34) Croutch, V. K.; Hartley, R. A. *J. Coatings Technol.* **1992**, *64*, 41-53.

(35) Andersson, L. O.; Golander, C. G.; Persson, S. *Fuel Sci. Technol. Int.* **1994**, *12*, 117-132..

(36) Wei, Y.; Adamson, R. M.; Dempsey, J. P. *J. Mater. Sci.* **1996**, *31*, 943-947.

(37) Saito, H.; Takai, K.; Yamauchi, G. *Surf. Coat. Int.* **1997**, *80*, 168-171.

(38) Pittenger, B.; Cook, D. J.; Slaughterbeck, C. R.; Fain, S. C., Jr. *J. Vac. Sci. Technol., A* **1998**, *16*, 1832-1837.

(39) Archer, P.; Gupta, V. *J. Mech. Phys. Solids* **1998**, *46*, 1745-1771.

(40) Ryzhkin, I. A.; Petrenko, V. F. *J. Phys. Chem. B* **1997**, *101*, 6267-6270.

(41) Petrenko, V. F. *J. Phys. Chem. B* **1997**, *101*, 6276-6281.

(42) Petrenko, V. F.; Whitworth, R. W. *Physics of Ice*; Oxford University Press: New York, NY, 1999.

(43) Petrenko, V. F.; Peng, S. *Can. J. Phys.* **2003**, *81*, 387-393.

(44) Somlo, B.; Gupta, V. *Mech. Mater.* **2001**, *33*, 471-480.

(45) Kako, T.; Nakajima, A.; Irie, H.; Kato, Z.; Uematsu, K.; Watanabe, T.; Hashimoto, K. *J. Mater. Sci.* **2004**, *39*, 547-555.

(46) N. Bhate, M. Hsu, G. O'Neil, T. Deng, S. Okuyama, J. Stein, N. Turnquist, K. K. Varanasi, US 11/487023, EP 1750018, 2006.

(47) Zwieg, T.; Cucarella, V.; Kauffeld, M. *Int. J. Mater. Res.* **2007**, *98*, 597-602.

(48) Akitegetse, C.; Volat, C.; Farzaneh, M. *Meas. Sci. Technol.* **2008**, *19*, 065703/1-065703/9.

(49) Holberg, S.; Cucarella, V.; Ramloev, H.; Tur, G.; Worch, H.; Zwieg, T. *Pitture Vernici, Eur. Coat.* **2008**, *84*, 25/68-29/68, 31/68-32/68.

(50) Cao, L.; Jones, A. K.; Sikka, V. K.; Wu, J.; Gao, D. *Langmuir* **2009**, *25*, 12444-12448.

(51) Dotan, A.; Dodiuk, H.; Laforte, C.; Kenig, S. *J. Adhes. Sci. Technol.* **2009**, *23*, 1907-1915.

(52) Kulinich, S. A.; Farzaneh, M. *Appl. Surf. Sci.* **2009**, *255*, 8153-8157.

(53) Kulinich, S. A.; Farzaneh, M. *Langmuir* **2009**, *25*, 8854-8856.

(54) Menini, R.; Farzaneh, M. *Surf. Coat. Technol.* **2009**, *203*, 1941-1946.

(55) Sarkar, D. K.; Farzaneh, M. *J. Adhes. Sci. Technol.* **2009**, *23*, 1215-1237.

(56) Wang, F. C.; Li, C. R.; Lv, Y. Z.; Lv, F. C.; Du, Y. F. *Cold Reg. Sci. Technol.* **2010**, *62*, 29-33.

(57) Menini, R.; Ghalmi, Z.; Farzaneh, M. *Cold Reg. Sci. Technol.* **2010**, *In Press*.

(58) Kulinich, S. A.; Farzaneh, M. *Cold Reg. Sci. Technol.* **2010**, *In Press*.

(59) Della Volpe, C.; Siboni, S.; Morra, M. *Langmuir* **2002**, *18*, 1441-1444.

(60) Gao, L. C.; McCarthy, T. J. *Langmuir* **2008**, *24*, 9183-9188.

(61) Gao, L. C.; McCarthy, T. J. *Langmuir* **2009**, *25*, 14105-14115.

(62) Furmidge, C. G. *J. Colloid Sci.* **1962**, *17*, 309-324.

(63) Johnson, R. E., Jr.; Dettre, R. H. In *Wetting of Low Energy Surfaces*, Marcel Dekker: New York, NY, 1993; pp 2-71.

(64) Young, T. *Philos. Trans. R. Soc. London* **1805**, *95*, 65.

(65) Dupré, A. *Théorie Mécanique de la Chaleur*; Gauthier-Villars, **1869**.

(66) Hiemenz, P. C.; Rajagopalan, R. *Principles of Colloid and Surface Chemistry*, 3rd ed.; Marcel Dekker: New York, NY, 1997.

(67) Mittal, K. L. In *Adhesion Measurement of Thin Films, Thick Films and Bulk Coatings*; ASTM Special Tech. Publ. 640: Philadelphia, PA, 1976; pp 5-16.

(68) Pocius, A. *Adhesion and Adhesive Technology*, 2nd ed.; Carl Hanser Verlag: Münich, Germany, 2002.

(69) De Souza, E. J.; Gao, L. C.; McCarthy, T. J.; Arzt, E.; Crosby, A. J. *Langmuir* **2008**, *24*, 1391-1396.

(70) Jellinek, H. H. *J. Appl. Phys.* **1961**, *32*, 1793-1794.

(71) Wenzel, R. N. *J. Ind. Eng. Chem.* **1936**, *28*, 988-994.

(72) Cassie, A. B. D.; Baxter, S. *Trans. Faraday Soc.* **1944**, *40*, 546-551.

(73) Tuteja, A.; Choi, W.; Mabry, J. M.; McKinley, G. H.; Cohen, R. E. *Proc. Natl. Acad. Sci. U. S. A.* **2008**, *105*, 18200-18205.

(74) Mabry, J. M.; Vij, A.; Iacono, S. T.; Viers, B. D. *Angew. Chem. Int. Ed.* **2008**, *47*, 4137-4140.

(75) Tuteja, A.; Choi, W.; Ma, M.; Mabry, J. M.; Mazzella, S. A.; Rutledge, G. C.; McKinley, G. H.; Cohen, R. E. *Science* **2007**, *318*, 1618-1622.

(76) Choi, W.; Tuteja, A.; Chhatre, S.; Mabry, J. M.; Cohen, R. E.; McKinley, G. H. *Adv. Mater.* **2009**, *21*, 2190-2195.

(77) Chhatre, S. S.; Tuteja, A.; Choi, W.; Revaux, A.; Smith, D.; Mabry, J. M.; McKinley, G. H.; Cohen, R. E. *Langmuir* **2009**, *25*, 13625-13632.

(78) Chhatre, S. S.; Choi, W.; Tuteja, A.; Park, K.; Mabry, J. M.; McKinley, G. H.; Cohen, R. E. *Langmuir* **2010**, *26*, 4027-4035.

(79) Marmur, A. *Soft Matter* **2006**, *2*, 12-17.

(80) Della Volpe, C.; Brugnara, M.; Maniglio, D.; Siboni, S.; Wangdu, T. In *Contact Angle, Wettability and Adhesion, Vol. 4*; VSP: Boston, MA, 2006; pp 79-99.

(81) Andrieu, C.; Sykes, C.; Brochard, F. *Langmuir* **1994**, *10*, 2077-2080.

(82) Della Volpe, C.; Maniglio, D.; Siboni, S.; Morra, M. *Oil & Gas Sci. and Tech.* **2001**, *56*, 9-22.

(83) Bangham, D. H.; Razouk, R. I. *Trans. Faraday Soc.* **1937**, *33*, 1459-1462.

(84) Beamson, G.; Briggs, D. *High Resolution XPS of Organic Polymers: The Scientia ESCA300 Database;* Wiley: New York, NY, 1992.

(85) Owen, M. J.; Kobayashi, H. *Macromol. Symp.* **1994**, *82*, 115-123.

(86) K. K. Varanasi, M. Hsu, N. Bhate, W. Yang, T. Deng, *Appl. Phys. Lett.* **2009**, *95*, 094101.